Acoustics of pianos: physical modeling, simulations and experiments

Antoine Chaigne, Juliette Chabassier, Nicolas Burban

Acoustics of pianos: physical modeling, simulations and experiments

Antoine Chaigne
UME, Ensta ParisTech, France
antoine.chaigne@ensta.fr

Juliette Chabassier
Poems Team, Inria, France
juliette.chabassier@inria.fr

Nicolas Burban
Ecole polytechnique, France
nicolas.burban@polytechnique.edu

ABSTRACT

The outlines of a recently developed model of a grand piano are summarized. Using dedicated numerical methods, the main vibratory and acoustic variables of each constitutive part of the instrument (strings, bridge, soundboard, sound pressure) are simulated in the time-domain. The obtained waveforms are analyzed and compared with experimental data derived from measurements on a Steinway D grand piano. This comparison yields valuable insight into the physics of the instrument. It shows, in particular, that a nonlinear string model is necessary to account for the observed richness of piano spectra. The model is able to reproduce important features of piano sounds, such as the presence of soundboard modes in the transients, precursors and phantom partials. However, one important limitation of the model, in its present state, is that it does not account for the change of polarization observed on piano strings. Experimental observations of this phenomenon are discussed and a preliminary model for explaining the possible role of the zig-zag end condition in string polarization change is presented.

1. INTRODUCTION

A piano model has been recently developed that couples together the hammer, the strings, the soundboard and the air [1]. One particularity of this model is that it is based on a nonlinear description of string motion. As a consequence, an original model of string-soundboard coupling at the bridge is developed, in order to allow transmission of both transverse and longitudinal forces to the soundboard. This implies to elaborate dedicated numerical schemes in order to ensure stability, and to satisfy the strong requirements of musical sound synthesis in terms of dispersion [2] [3]. Since both the model and the associated numerical methods are extensively described elsewhere, only a brief summary is given in Section 2. In Section 3, some selected results of simulations are analyzed both in the time and frequency domains, where the influence of string amplitude in the resulting sounds is highlighted. Comparison with experimental waveforms and spectra shows that the model is able to reproduce the precursors, the phantom partials and the presence of soundboard modes observed in recorded piano tones. However, in its present state, the model is not capable to account for the time evolution of the string's polarization plane observed in most pianos. In Section 4, a mixed experimental-numerical preliminary study is reported whose aim is to examine whether the usually observed and so-called "zig-zag" end conditions can be responsible for such changes in polarization. These changes are important since they affect the temporal envelope of the tones and are clearly audible.

2. A PIANO MODEL

2.1 Summary of the model

The model allows to calculate the sound of a piano in the time-domain, from the starting time where the hammer hits the strings, initially at rest, with a given velocity. The key mechanism that transmits the player's action from the keyboard to the hammer is ignored. It is considered to include it in future versions. One major feature of the model is that the geometrical nonlinearity the strings, due to large displacements, is taken into account in addition to stiffness. The model allows the transmission of these nonlinearities from strings to soundboard at the bridge. This yields, among other things, the possibility of simulating phantom partials and precursors [4]. The hammer is defined as a dissipative nonlinear spring [5]. The motion of the strings is governed by nonlinear wave propagation equations, accounting for the large displacement that can be observed especially during the attack [6]. This geometrical nonlinearity induces a coupling between the transverse and the longitudinal polarizations of the strings. This coupling has many consequences on the spectral content, and also on the temporal envelopes of the sounds. The string stiffness is modeled by a Timoshenko model, which has better physical and mathematical properties than the Euler-Bernoulli model. The string model is written:

Boundary condition (agraffe side $x = x_a$): (1)

$$u_s(x = x_a, t) = v_s(x = x_a, t) = \frac{\partial \varphi_s}{\partial x}(x = x_a, t) = 0,$$

Initial conditions: (2)

$$\begin{cases} u_s(x, t = 0) = v_s(x, t = 0) = \varphi_s(x, t = 0) = 0, \\ \frac{\partial u_s}{\partial t}(x, t = 0) = \frac{\partial v_s}{\partial t}(x, t = 0) = \frac{\partial \varphi_s}{\partial t}(x, t = 0) = 0. \end{cases}$$

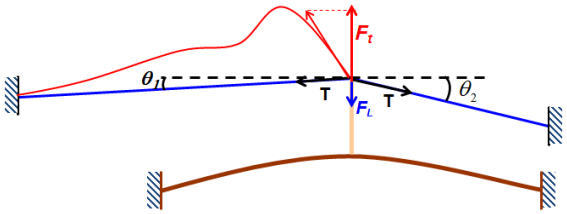

Figure 1. String-soundboard coupling. The force transmitted from string to soundboard has two components. F_t is due to the transverse motion of the string, while F_L is due to its longitudinal motion.

Nonlinear stiff string motion:

$$\begin{cases} \rho A \dfrac{\partial^2 u_s}{\partial t^2} - \dfrac{\partial}{\partial x}\left[EA \dfrac{\partial u_s}{\partial x} - \dfrac{(EA - T_0)\dfrac{\partial u_s}{\partial x}}{\sqrt{\left(\dfrac{\partial u_s}{\partial x}\right)^2 + \left(1 + \dfrac{\partial v_s}{\partial x}\right)^2}} \right] \\ \quad + AG\kappa \dfrac{\partial}{\partial x}\left(\varphi_s - \dfrac{\partial u_s}{\partial x}\right) = S, \\ \rho A \dfrac{\partial^2 v_s}{\partial t^2} - \dfrac{\partial}{\partial x}\left[EA \dfrac{\partial v_s}{\partial x} - \dfrac{(EA - T_0)\left(1 + \dfrac{\partial v_s}{\partial x}\right)}{\sqrt{\left(\dfrac{\partial u_s}{\partial x}\right)^2 + \left(1 + \dfrac{\partial v_s}{\partial x}\right)^2}} \right] \\ \quad = 0, \\ \rho I \dfrac{\partial^2 \varphi_s}{\partial t^2} - EI \dfrac{\partial^2 \varphi_s}{\partial x^2} + AG\kappa \left(\varphi_s - \dfrac{\partial u_s}{\partial x}\right) = 0 \end{cases} \tag{3}$$

where u_s is the vertical transverse displacement of the string, v_s is the longitudinal displacement, and φ_s is the angle of the cross-sections with the plane normal to the string. The source term S represents the action of the hammer. For clarity, the additional fluid and viscoelastic-like damping terms are not written in Equation (3). The string-soundboard coupling at the bridge is modeled in such a way that both the transverse and longitudinal components of the strings are transmitted to the soundboard. This is obtained by considering that the string is slightly bent due to both the bridge height and soundboard curvature (see Figure 1). As a result, the vibration spectrum of the soundboard (velocity or acceleration) has a full richness, comparable to real tones. The soundboard is modeled as a flat orthotropic Reissner-Mindlin plate of variable thickness [1]. The ribs and the bridge are modeled as local heterogeneities in terms of thickness and elasticity (see Figure 2). The parameters of the soundboard (size, materials and thickness profile) are adjusted with great accuracy, in order to allow comparison with existing soundboards. The number and location of ribs can be adjusted so that comparisons can be made between the sounds produced for various configurations of the soundboard. The 3D sound field around

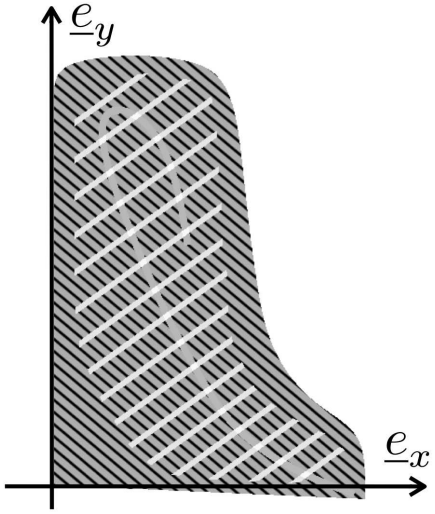

Figure 2. Soundboard model. The black lines indicate the direction of the fibers. The white lines represent the ribs. The grey curve is the bridge.

the instrument is computed in a virtual box bounded by absorbing boundary conditions (or Perfectly Matched Layers), thus simulating a free space as in an anechoic chamber [7]. The rim is taken into account as a rigid obstacle for the sound waves, but its vibrations are ignored. The coupling between the soundboard and the sound field is governed by the continuity of the normal velocity on the soundboard surface, as done for previous modeling of timpani [8] and guitar [9].

2.2 Summary of the numerical methods

Specific methods are used for the discretization of each subsystem and of the coupling terms. To ensure long-term stability, the numerical schemes are based on the formulation of a discrete energy, consistent with the continuous energy of the considered system, which is either constant or decreasing with time. In addition, the discrete formulation of the coupling terms is conservative and fulfils the reciprocity principle. For the strings, two different schemes were adopted: one for the linear part, and another one, specifically developed [2], for the nonlinear part. This new scheme is applicable to a special class of equations called "Hamiltonian system of wave equations". For the linear part, two different implicit θ-schemes are used: one, conditionally stable with reduced dispersion, for the transverse wave, and another one, unconditionally stable, for both the longitudinal and shear waves. Although the numerical dispersion is higher in this latter case, it has only little consequences since most partials of these waves are beyond the audio range. The stability condition applicable to the linear part yields a condition for the time step, which is selected here equal to Δt=10^{-6} s. For the hammer-string coupling, a nonlinear three time steps formulation is used. For the soundboard, a modal decomposition is made once for all (for given geometry and material properties) followed by a semi-analytic time resolution of the obtained

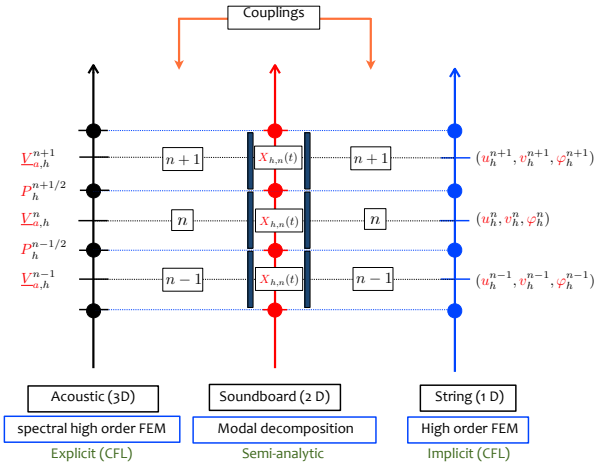

Figure 3. The discretization scheme of the piano model is summarized. The three discrete components of the strings'motion (u_h, v_h, φ_h) and the acoustic velocity $V_{a,h}$ are calculated on the time grid $n\Delta t$. The soundboard modal displacements $X_{h,p}$ and the sound pressure P_h are calculated on the time grid $[n + 1/2]\Delta t$ so as to ensure conservation of the discrete energy.

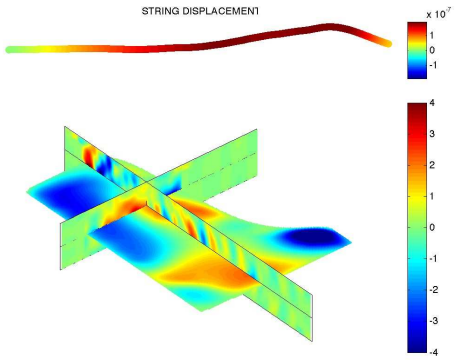

Figure 4. Example of computation for the note C2, at time t=3.21 ms after the attack. The figure at the top shows the transverse shape of the string displacement, while the longitudinal component is represented by a color scale within the string. The figure at the bottom shows the displacement of the soundboard and the pressure field in two planes perpendicular to the soundboard crossing at the attachment point of string C2 on the bridge. The lower scale refers to the sound pressure (in Pa).

set of second-order differential equations, where damping is added mode by mode, as done in the past for the guitar [9]. This amounts to assuming that the modal damping matrix is diagonal. The values of the damping terms are extracted from the existing literature and from our own measurements. In practice, 2400 modes have to be calculated for a Steinway D soundboard in the range 0 to 10 kHz. The string-soundboard coupling equations at the bridge are obtained by considering the continuity of the vertical velocity and nullity of the horizontal velocity at the bridge for both subsystems. This allows to couple the discrete string scheme with the semi-analytic soundboard model. In practice, the strings and soundboard unknowns are evaluated on interleaved grids: $\{n\Delta t\}$ for the strings, and $\{n + 1/2\Delta t\}$ for the soundboard (see Figure 3). Finally, for the acoustic propagation, higher-order finite-elements are used. The acoustic space is artificially bounded by Perfectly Matched Layers [7]. Again, the acoustic velocity and sound pressure are evaluated on interleaved grids (see Figure 3). Figure 4 shows an example of computation for the note C2, at time $t = 3.21$ ms after the hammer blow. The upper figure shows the transverse string displacement, while the longitudinal displacement is represented by a color scale within the string. The lower figure shows together the displacement of the soundboard and the pressure field in two planes perpendicular to the soundboard and crossing at the attachment point of the C2-strings on the bridge.

3. ANALYSIS OF SIMULATIONS

3.1 Frequency domain: phantoms and soundboard modes

The effects of transverse-longitudinal coupling in string motion can be seen in Figure 5 which shows the spectrum of the longitudinal component of string F3 (fundamental $f_1 = 175$ Hz), for soft (piano) and strong (forte) hammer blow. The soft attack corresponds to an initial hammer velocity V_H=0.5 m/s, leading to a maximum amplitude of the string's displacement equal to 0.34 times its diameter. For the strong attack, we have V_H=3 m/s, and a maximum amplitude to diameter ratio equal to 2.1. In both cases, the dominant frequency is the fundamental longitudinal frequency at 2.64 kHz. The coupling is attested by the presence of transverse components in the spectra. As expected, the density of phantom partials is higher for the strong attack. These partials can be seen as additional components between the transverse components, especially in the range 2 to 4 kHz. Accurate frequency analysis shows that the frequencies of these partials are combinations of transverse and longitudinal frequencies due to quadratic and cubic nonlinearities, and are governed by simple arithmetic rules [1]. However, the question of existence of such partials is not trivial and requires a thorough stability analysis [10]. Similar phenomena are observed in other percussive instruments subjected to geometrical nonlinearities, such as gongs and cymbals [11]. Most of these frequencies could not be seen in the case of string without stiffness. They become visible because of the inharmonicity due to stiffness. As stated above, the relative magnitude of both these longitudinal and phantom frequencies in soundboard vibrations and sound pressure critically depend on the coupling conditions at the bridge. Examples of simulated sound pressure spectra are shown in Figure 6 for three different hammer impact velocities corresponding to piano, mezzo-forte and forte playing. Added components below 1 kHz are present, with identical frequencies and similar relative magnitude with regard to the string's partials in all three cases. Accurate spectral analysis shows that these components correspond to soundboard modes.

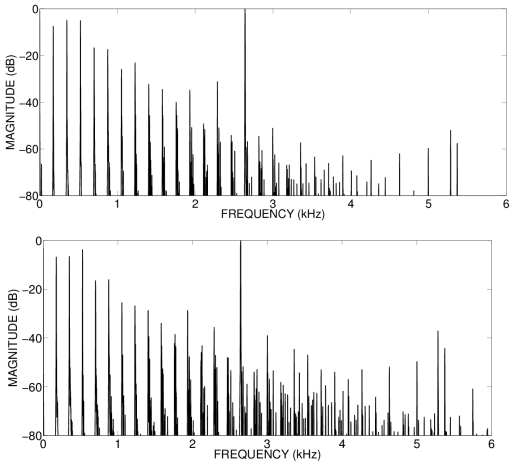

Figure 5. Spectrum of the simulated longitudinal component of the F3 string's displacement for soft (top) and strong (bottom) attack. The longitudinal frequency (at 2.64 kHz) is dominant, and phantom partials can be seen even for a soft attack. The pressure scaling at 0 dB is obtained by taking the magnitude of the strongest partial as reference.

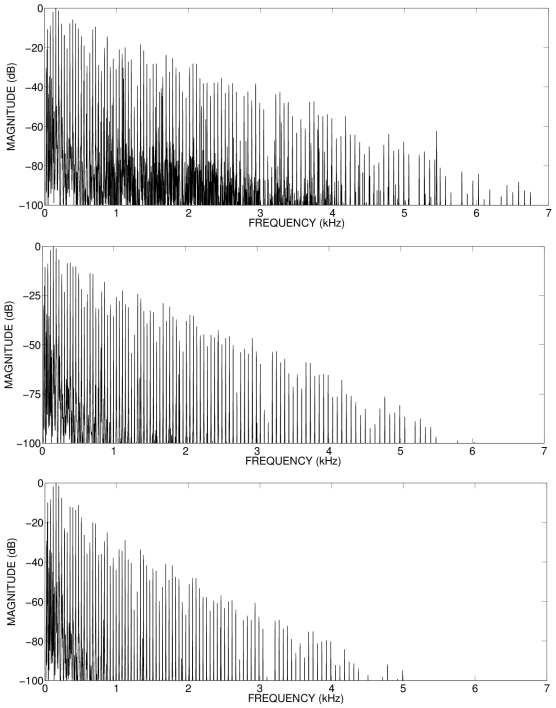

Figure 6. Spectra of simulated sound pressure in the piano near field. Note D♯1 (single string) at three different levels: forte (V_H=3 m/s ; top), mezzo-forte (V_H=1.5 m/s ; middle) and piano (V_H = 0.5 m/s ; bottom). The pressure scaling at 0 dB is obtained by taking the magnitude of the strongest partial as reference. The spectra are averaged during the first 1.6 s of the sound.

The total bandwidth (within a dynamic range of 100 dB) increases with the initial hammer velocity, from 5 kHz, for the "piano"touch", to 7 kHz for the "forte" touch. This effect is due to the nonlinearity of the hammer felt. Between 1 and 5 kHz, the nonlinearity of the string is responsible for additional frequencies situated between the string's partials and visible as black regions in Figure 6. These frequencies are the so-called "phantom" partials due to the presence of quadratic and cubic terms in the Taylor expansion of both the transverse and longitudinal string force. Zooming on these zones allow accurate measurements of these phantom frequencies, who correspond to combinations (sums and differences) of the eigenfrequencies of the string [1]. In the "forte" case, for this string D♯1, the amplitude of the phantoms is particularly high around 1.2, 1.7, 2.3, 2.8, 3.3, 3.7 and 3.9 kHz. The comparison of Figure 6 with the spectral analysis of sound pressure recorded in the vicinity of a Steinway D grand piano shows similar aspects and some differences. The presented spectra are obtained with three successive attacks, from "piano" to "forte". In this case the hammer velocity was not measured, but the experimentally observed hammer forces are comparable to the simulations. Again, soundboard modes are visible in the low-frequency range (below 800 Hz). The total bandwidth also increases from bottom (soft impact) to the top (strong impact). However, the bandwidth is reduced, compared to the simulations, growing from 3 to 5.5 kHz (for a dynamic range equal to 100 dB). This discrepancy might be due to an underestimation of the internal damping in strings and soundboard, and/or underestimation of the radiated sound power. In the low-frequency range, it is hard to isolate the vibrations of the soundboard from the rest of the instrument. Therefore, it is perfectly conceivable that a part of the soundboard energy is being transmitted to other elements, such as the rim. Phantom partials are also observed in the three cases, with increasing relative amplitudes from "piano" to "forte" sounds. Maxima of the phantoms amplitudes are observed around 1.2, 1.7, 2.0, 2.3, 2.8, 3.3 and 3.9 kHz, which is very similar to the situation observed in the simulations. One main difference here is that the level of the phantoms are significant, even for a soft impact. This might be either due to differences in bridge transmission and/or to higher string amplitude than in the model. Further work is needed here for explaining these results.

3.2 Time-domain: precursors

The effect of string amplitude is also visible in the time-domain on the pressure waveforms (see Figure 8). The small precursor observed for a soft impact is due to the physical dispersion consecutive to string's stiffness. The amplitude of the precursor increases with hammer velocity, and its spectral content changes: frequency analysis shows a spectrum comparable (mutatis mutandis for D♯1) to the longitudinal component in Figure 5 with a noticeable longitudinal fundamental frequency at 544 Hz. The consequence of decreasing bandwidth is visible on the waveforms which become smoother as the initial hammer velocity decreases. Such observations can be made for both measured and simulated pressure waveforms. Comparison between measurements and simulations show that the positions and relative magnitudes of the main pulses are fairly well reproduced, although the details of the wave-

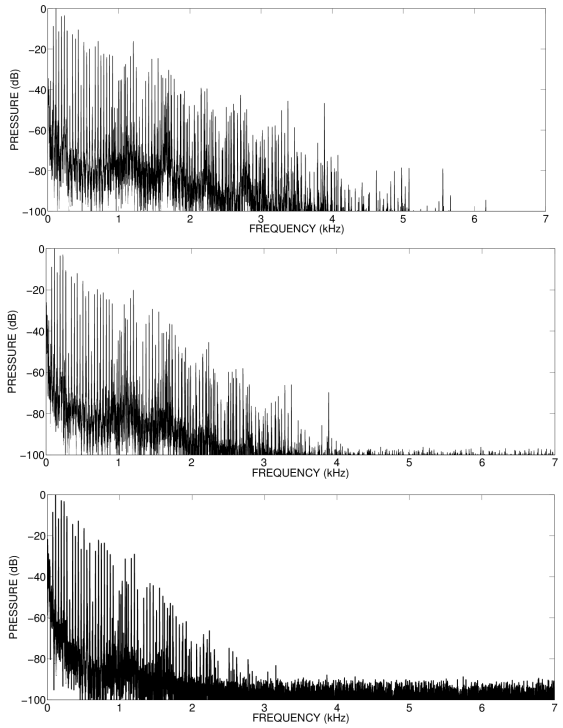

Figure 7. Spectra of measured sound pressure in the vicinity of a Steinway D grand piano. Note D♯1 (single string) at three different levels: forte (top), mezzo-forte (middle) and piano (bottom). The pressure scaling at 0 dB is obtained by taking the magnitude of the strongest partial as reference. The spectra are averaged during the first 1.6 s of the sound.

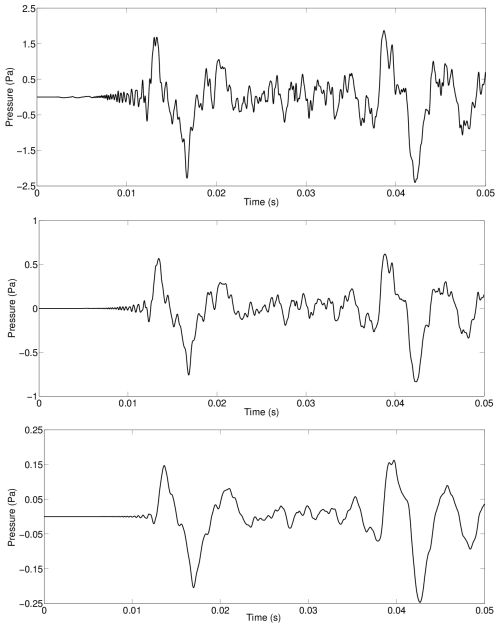

Figure 8. Simulation D♯1. Pressure waveforms during the first 50 ms of the sound. Same hammer velocities as in Figure 6. (Top) forte ; (middle) mezzo-forte ; (bottom) piano.

forms differ. This might be due to phase shifts, since the exact location of the microphone is not perfectly known. More experiments are necessary to check the pertinence of this assumption.

4. BOUNDARY CONDITIONS AT THE BRIDGE

4.1 Experiments

One important limitation of the above presented model is due to the fact that it does not allow any exchange of energy between the two transverse components of the string. As shown in Figure 10, such exchange is currently observed on pianos, even for single strings. Assuming perfect constant circular cross-section and homogeneity, then such exchange can only be driven by the boundary conditions. In this study, we made the *a priori* hypothesis that energy exchange can be due to two essential mechanisms: a rocking motion of the bridge, and particular geometry of the string-bridge contact. In order to isolate both mechanisms, a special monochord has been designed on purpose: it consists of a single string passing over a piece of wood representing a portion of "bridge" and glued on an arched flexible beam that plays the role of the "soundboard". Two photodetectors HOA1877 situated close to the string end deliver signals proportional to the two transverse components of the string's displacement. The strings are excited by the blow of mallets with variable hardness. A first preliminary series of experiments is conducted with a "V-shaped" boundary condition, where the "V" is situated in the symmetry plane of the "bridge" (see Figure 11). This prevent us against any change of polarization due to rocking motion of the bridge. As expected, the result shows that a vertical blow induces a vertical motion of the string and that no horizontal component is observable during the 5 s decay (see Figure 12). Another series of experiments is conducted with a so-called "zig-zag" end conditions observed on many pianos. It consists in two needles embedded in the bridge apart from one another in the direction of the string, forming an angle α with the vertical plane in opposite directions (see Figures 13 and 15). Here again, the holes for the needles are drilled in the symmetry plane of the bridge, so as to prevent any influence of rocking motion. In this case, the presence of a horizontal component is observed in the string motion after some time. The energy exchange varies with the angle α. For $\alpha = 90$ degrees, the end of the string is blocked. For $\alpha = 0$, the situation is particular since the string is not fixed at all. In both cases, an initial vertical blow does not induce any horizontal component. For intermediate values, typically for α within the range 20 to 60 degrees, then an horizontal component clearly appears (see Figure 14).

4.2 Modeling and simulation

A simple model of the zig-zag end condition is built as an attempt to explain the observed change of polarization of the string. As shown in Figure 15, the string is allowed to move along the needle. The model also allows a possible loss of contact between the string and the needle. In the absence of friction, the reaction of the needle is perpendicular to it. The model is tested first without friction

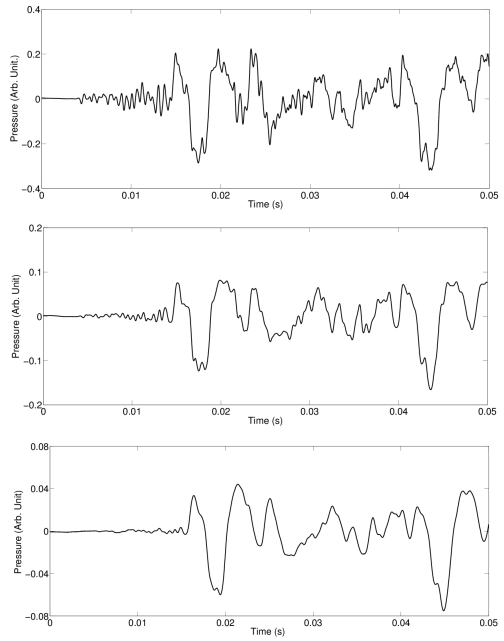

Figure 9. Measurements D♯1. Steinway D. Recorder pressure waveforms during the first 50 ms of the sound. Similar hammer forces as in Figure 8. (Top) forte ; (middle) mezzo-forte ; (bottom) piano.

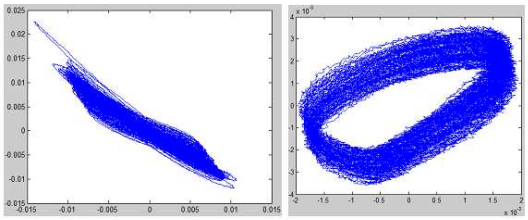

Figure 10. Observed change of polarization on a piano string. The photodetectors form an angle of 45 ° with the vertical plane. The left figure shows the vertical motion of the string just after the blow, while the right figure shows its horizontal motion after several seconds.

and secondly with a friction force that limits the possibility of slipping along the needle. To simplify the model, the speaking length of the string is represented by a mass-spring system composed of two identical masses M and N, and three springs of identical stiffness (see Figure 16). These lumped parameters are adjusted so as the eigenfrequencies of this 2-dof system are of the order of magnitude of the first partials of the continuous string. The masses are allowed to move in the x, y and z directions, although the z-component (longitudinal motion) can be neglected compared to the two others (see Figure 15). The first bend of the zig-zag end condition is modeled at point Z. A last spring with same stiffness as in the lumped string is simulated between Z and the point P. This last point represents the second bend of the zig-zag and is assumed to be fixed. The model is solved numerically using finite differences for the differential equations of the oscillators, and a predictor-corrector method for the boundary conditions. A typical result can be seen in Figure 17 showing the motion of the mass M. An initial vertical velocity is imposed (string motion in blue). The polarization axis then turns progressively (motion in green). After some time, the locus of the mass is elliptic (in red) and the orientation of the largest axis of the ellipse remains constant. The simulations show in addition that the main axis of this ellipse remains closer to the vertical axis if the angle α increases. This is coherent with the experimental observations. The horizontal component shown in this simulation is about three times larger than the one observed in Figure 14. This might be due to the fact that we observe here the motion of a point at one-third of the string, whereas the experimental data were recorded close the end, because of limited linearity range of the photodetectors. More accurate simulations must be conducted with a larger number of lumped elements in order to compare better the results with the experiments. The simulation of the string's motion at point Z under the needle shows that this point slips most of the time along the needle (in green), with a few erratic jumps (los of contact) of small amplitude at the end of the sequence

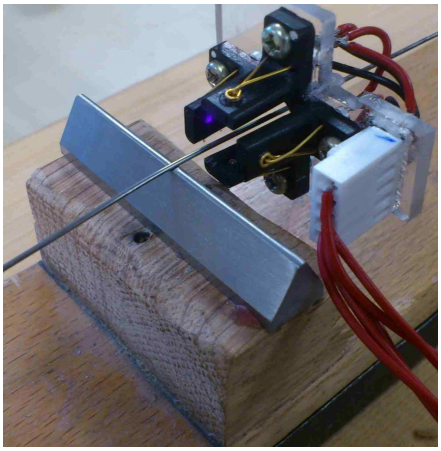

Figure 11. Experimental set-up showing the string, the photodetectors, the V-shaped boundary condition, the bridge and the beam.

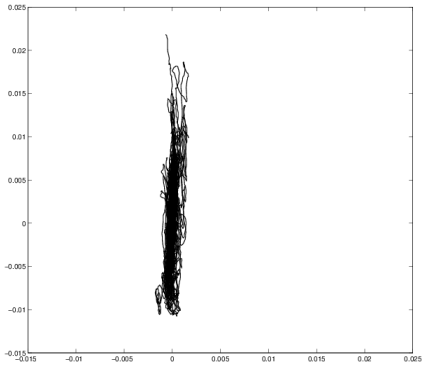

Figure 12. Constant polarization of the string observed for a V-shaped boundary condition place in the symmetry axis of the bridge. The photodetectors are situated in the vertical and horizontal planes, respectively. The duration of the observed decay is 5 s.

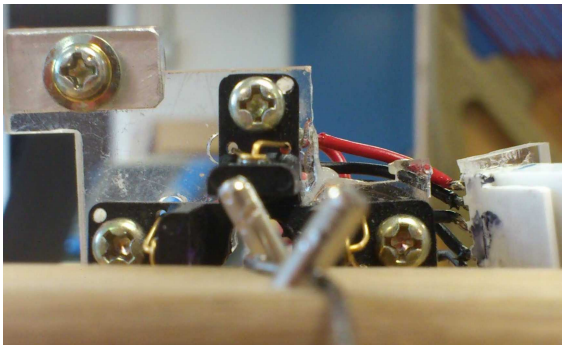

Figure 13. Zig-zag end condition.

(see Figure 18). One conclusion from this simple model is that the string might be subjected to micro-slipping at the zig-zag end at each arrival of the transverse pulses. The amplitude of these slipping depend on the friction. As a consequence, the string progressively takes an horizontal transverse component, and thus its polarization changes. In a piano, this horizontal component "sees" an input admittance at the bridge which is usually much higher than the admittance seen by the transverse vertical component. As a result, the vertical component is damped quicker and the horizontal component is dominant at the end of the tone.

5. CONCLUSION

The presented model of a grand piano is able to reproduce the main features of piano sounds and vibrations. The nonlinear string model and the string-soundboard coupling, in particular, account for both the dependence of tone quality upon string amplitude and transmission of longitudinal components to the rest of the instrument. This allows us to simulate the spectral richness of piano sounds efficiently, including the presence of soundboard modes and phantom partials. The frequencies of these partials are predicted with great accuracy. However, some discrepancies exist on the prediction of their amplitudes, which incites us to reconsider the string-soundboard coupling conditions at the bridge in the future. Auditory evaluation of the simulated sound pressure shows, in addition, that the model fails in reproducing the bass/treble balance of the lowest notes accurately. More investigations are needed at this stage to properly evaluate the internal causes of losses in strings and soundboard, and reconsider the possible transmission of energy from the soundboard to other parts of the body (rim, keybed) in this frequency range. Another limitation of the model is that it does not allow energy exchange between the two transverse polarizations of the string. The experiments and simulations presented here show that the zig-zag end condition settled on many pianos might be a cause for such exchange. With the help of a simple lumped model, we were able to reproduce, at least qualitatively, the main properties observed on real strings. The rocking motion of the bridge also might a possible candidate at the origin of polarization change: its influence will be examined in the near future.

Acknowledgments

The authors wish to thank Lahcène Cherfa for the development of the monochord, Marc Duruflé for his valuable help in the simulations, and René Caussé for making the Steinway D piano available to us for the measurements.

6. REFERENCES

[1] J. Chabassier, A. Chaigne, and P. Joly, "Modeling and simulation of a grand piano," *J. Acoust. Soc. Am.*, 2013, (submitted).

[2] J. Chabassier and P. Joly, "Energy preserving schemes for nonlinear Hamiltonian systems of wave equations. Application to the vibrating piano string." *Computer Methods in Applied Mechanics and Engineering*, vol. 199, pp. 2779–2795, 2010.

[3] J. Chabassier and S. Imperiale, "Stability and dispersion analysis of improved time discretization for simply supported prestressed Timoshenko systems. Application to the stiff piano string." *Wave Motion*, 2012.

[4] H. A. Conklin, "Generation of partials due to nonlinear mixing in a stringed instrument," *J. Acoust. Soc. Am.*, vol. 105, no. 1, pp. 536–545, 1999.

[5] A. Stulov, "Dynamic behavior and mechanical features of wool felt," *Acta Mechanica*, vol. 169, no. 1, pp. 13–21, 2004.

[6] P. Morse and K. Ingard, *Theoretical Acoustics*. Princeton, New Jersey: Princeton University Press, 1968, ch. 14, pp. 856–863.

[7] E. Bécache, S. Fauqueux, and P. Joly, "Stability of perfectly matched layers, group velocities and anisotropic waves," *Journal of Computational Physics*, vol. 188, pp. 399–403, 2003.

[8] L. Rhaouti, A. Chaigne, and P. Joly, "Time-domain modeling and numerical simulation of a kettledrum," *J. Acoust. Soc. Am.*, vol. 105, pp. 3545–3562, 1999.

[9] G. Derveaux, A. Chaigne, P. Joly, and E. Bécache, "Time-domain simulation of a guitar: Model and method," *J. Acoust. Soc. Am.*, vol. 114, pp. 3368–3383, 2003.

[10] A. H. Nayfeh and D. T. Mook, *Nonlinear oscillations*, ser. Wiley classics library. Hoboken, New Jersey: J. Wiley, 1979.

[11] C. Touzé and A. Chaigne, "Lyapunov exponents from experimental time series: Application to cymbal vibrations," *Acustica united with Acta Acustica*, vol. 86, no. 3, pp. 557–567, 2000.

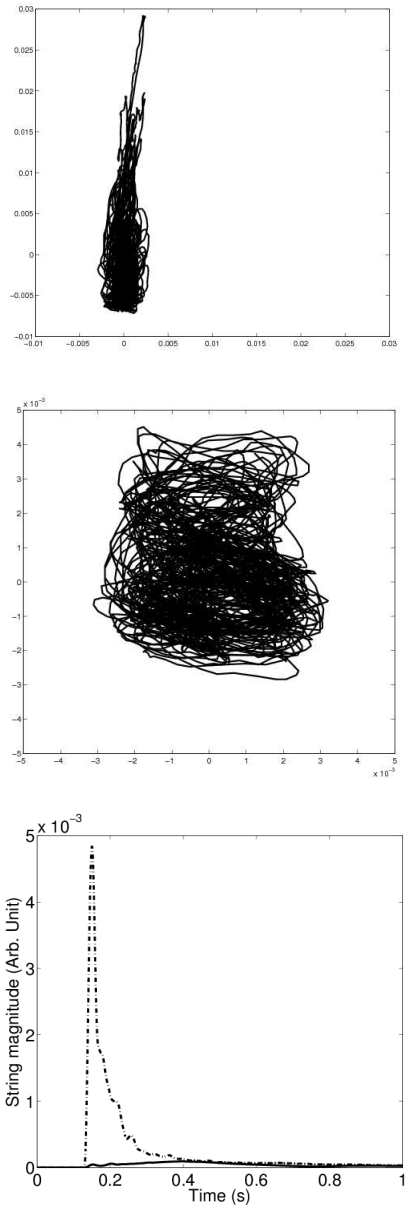

Figure 14. Zig-zag end condition. Comparison between string polarization during the first 100 ms (top) and after 0.35 s (middle) showing a progressive counterclockwise orientation of the axis to the string motion. The figure at the bottom displays the evolution of the envelope of both polarizations with time, showing a progressive increase of the horizontal component (solid line) during the first 200 ms of the string's oscillation. At time t=0.4 s, the magnitude of both components are comparable.

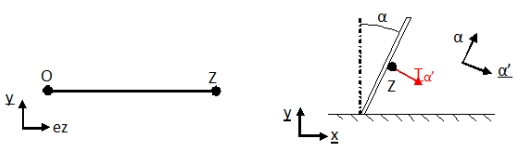

Figure 15. Model of the zig-zag end.

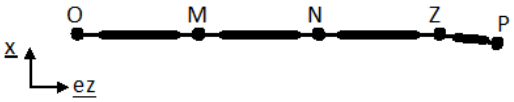

Figure 16. Discrete model of the string with one zig-zag end condition (top view).

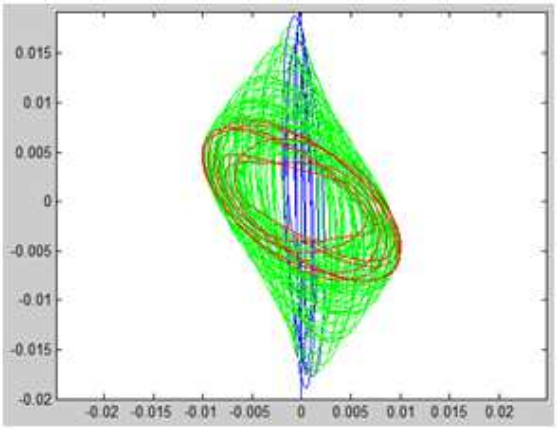

Figure 17. Simulated change of polarization of the simulated string with one zig-zag end. Motion of the mass M after the blow (in blue), during transition (in green), and after a few seconds (in red).

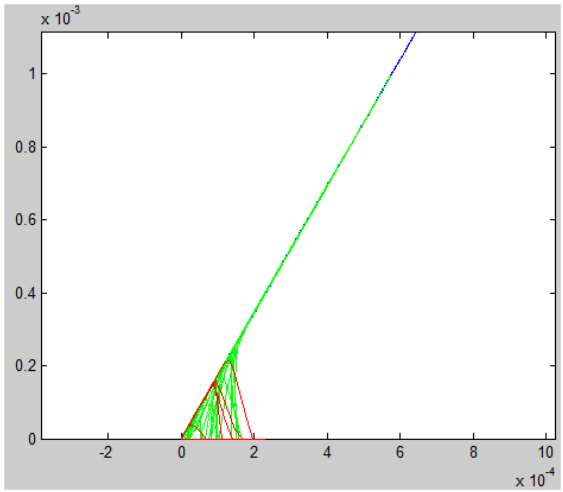

Figure 18. Simulated motion of the string close to the needle (Z-point in Figure 16).